Transmission-electron-microscopy study of quasi-epitaxial tungsten-bronze (Sr$_{2.5}$Ba$_{2.5}$Nb$_{10}$O$_{30}$) thin film on perovskite (SrTiO$_3$) single crystal

Dong Su, Anna Infortuna, Paul Muralt, and Nava Setter[a]
Ceramics Laboratory, Swiss Federal Institute of Technology (EPFL), Lausanne CH-1015, Switzerland

Marco Cantoni
Interdisciplinary Center for Electron Microscopy (CIME), Swiss Federal Institute of Technology (EPFL), Lausanne CH-1015, Switzerland

Strontium barium niobate (Sr$_{2.5}$Ba$_{2.5}$Nb$_{10}$O$_{30}$) thin films were deposited on (001) SrTiO$_3$ single-crystalline substrates by pulsed laser deposition. The growth nature was investigated by transmission electron microscopy (TEM). Selected-area electron diffraction and high-resolution transmission electron microscopy revealed the existence of six types of grains. These grains grew on the substrate in a partially epitaxial fashion. Geometrical models were built, which were confirmed by TEM observations. Based on the TEM results and geometrical analysis, a crystallographic model was developed. The strain nature resulting from the growth columns is discussed in this report.

I. INTRODUCTION

The tungsten-bronze (TB) structure strontium barium niobate (Sr$_{5x}$Ba$_{5-5x}$Nb$_{10}$O$_{30}$, SBN$_x$) is a uniaxial ferroelectric at room temperature, and its monocrystals exhibit large piezoelectric, pyroelectric, and electro-optic coefficients.[1,2] The para-to-ferroelectric phase transition occurs in the temperature range from 333 to 523 K, depending on the compositional parameter x. The large spontaneous polarization along the unique c axis leads to a very strong dielectric anomaly. The relatively low critical temperature of SBN$_x$ makes it an excellent candidate for pyroelectric infrared detectors. In view of these excellent single-crystal properties, there is an interest in investigating SBN thin films for applications in electromechanical and optical microsystem.[3]

In this work, epitaxial growth of SBN$_x$ thin films is investigated. Currently, there is no commonly available TB crystalline substrate. The most commonly used substrates are (001) oriented perovskite single crystals, such as MgO (NaCl-tpye structure) and SrTiO$_3$, because they have very low lattice mismatch along the c axis of SBN$_x$.[4–8] Thus, the interesting question arises: How is the TB structure accommodated on (001) perovskites? Growth of SBN$_{x=0.56}$ and SBN$_{x=0.61}$ on (100) MgO single crystals was studied by Thony et al. and

C.M. Rouleau et al., respectively.[6,7] Their results show the growth relationship to be SBN$_x\langle100\rangle$//MgO$\langle310\rangle$. Tanaka and co-workers reported the same growth relationship SBN$_x\langle100\rangle$//STO$\langle310\rangle$ in SBN$_{x=0.5}$ thin film on (001) STO single crystal.[8] They also indicated that in the configuration of SBN$_x\langle100\rangle$//STO$\langle310\rangle$, the lattice mismatch calculated is less than 1%, while the mismatch for SBN$_x\langle100\rangle$//MgO$\langle310\rangle$ is −6.2%. STO is a more suitable substrate for SBN epitaxial growth because it has a smaller misfit strain than MgO. Although a growth relation of SBN$\langle100\rangle$//MgO$\langle310\rangle$ was reported in their work, the growth nature of a TB-type SBN on perovskite substrate is still unclear.

In this work, we deposited epitaxial SBN$_{x=0.5}$ (SBN50, SBN hereafter) thin films on (100) SrTiO$_3$ (STO) single crystals by pulsed laser deposition (PLD). The growth nature was investigated by transmission electron microscopy (TEM). According to the lattice parameters' relationship between SBN and STO, the growth models were built. By diffraction simulating, we were able to compare the TEM results and the prediction of our models. The growth mechanism was discussed in terms of the lattice-mismatch strain between the film and the substrate.

II. EXPERIMENTAL PROCEDURE

SBN thin films were deposited on (001) STO substrates by PLD with a KrF excimer laser (λ = 248 nm). The targets were prepared by mixing SrCO$_3$, BaCO$_3$, and Nb$_2$O$_5$ powders in acetone and calcined at 1373 K for

---

12 h in air. The deposition temperature was 1013 K in oxygen atmosphere of 200–400 mTorr. The laser energy and repetition rate were 200–400 mJ and 10 Hz, respectively. Atomic steps for $SrTiO_3$ (1% Nb doped) substrates were observed via atomic force microscopy (AFM) prior to deposition. The crystallization of SBN thin films was examined by reflection high-energy electron diffraction (RHEED), which showed a high degree of roughness on the film surface. The detailed experimental procedure can be found elsewhere.[9]

Cross-section samples of SBN thin films were cut along the [100] direction of STO. The cut slides were glued face to face by jointing SBN film surfaces. TEM specimens were prepared by mechanical grinding, polishing down to 25 μm, followed by Ar-ion milling with a Gatan-PIPS (Pleasanton, CA). Plane-view samples were prepared by similar methods from the substrate side. The conventional diffraction contrast images and diffraction patterns were obtained in a Philips CM20 TEM (Hillsboro, OR). High-resolution transmission electron microscopy (HRTEM) was taken using a CM-300 FEG TEM.

III. RESULTS AND DISCUSSION

A. Growth models

At room temperature, the unit cell lattice parameters are $a = b = 1.246$ nm and $c = 0.3952$ nm for SBN (No. 39-0265 in the Powder Diffraction File database) and $a = b = c = 0.3905$ nm for STO (No. 79-0174).[10,11] It can be seen that the value of c_{SBN} is close to the value of a_{STO}, which means that it is possible for SBN to grow epitaxially on STO substrate. On the other hand, the value of a_{SBN} is much larger than the value of a_{STO}. This arrangement would lead to growth of SBN on STO that is not completely epitaxial, unlike cube-on-cube growth in system of perovskite on perovskite. The relationships between lattice parameters of SBN and STO are:

$$|a_{STO}| \approx |c_{SBN}| \quad , \tag{1}$$

$$(|a_{STO}|)^2 + (3|a_{STO}|)^2 \approx (|a_{SBN}|)^2 \quad . \tag{2}$$

To minimize the interface energy, the lattice of the SBN film would have the maximum match with the STO substrate on the growth. Therefore, from a geometrical view, six types of possible growth models can be deduced. The relationships of the lattice vectors are as follows:

Model 1: $c_{SBN} \approx a_{STO}$, and $(3|b_{STO}|)^2 + (|c_{STO}|)^2$
    $\approx (|a_{SBN}|)^2$

Model 2: $c_{SBN} \approx a_{STO}$, and $(|b_{STO}|)^2 + (3|c_{STO}|)^2$
    $\approx (|a_{SBN}|)^2$

Model 3: $c_{SBN} \approx b_{STO}$, and $(3|a_{STO}|)^2 + (|c_{STO}|)^2$
    $\approx (|a_{SBN}|)^2$

Model 4: $c_{SBN} \approx b_{STO}$, and $(|a_{STO}|)^2 + (3|c_{STO}|)^2$
    $\approx (|a_{SBN}|)^2$

Model 5: $c_{SBN} \approx c_{STO}$, and $(3|a_{STO}|)^2 + (|b_{STO}|)^2$
    $\approx (|a_{SBN}|)^2$

Model 6: $c_{SBN} \approx c_{STO}$, and $(|a_{STO}|)^2 + (3|b_{STO}|)^2$
    $\approx (|a_{SBN}|)^2$

The illustrations of these models are shown in Figs. 1(a)–1(c). In models 1–4, the c axis of SBN grows along the a or b axis of STO, and at the same time, the a or b axis of SBN tilts 18.4° away from the interface of the SBN and STO. In models 5 and 6, the c axis of SBN grows along the c axis of STO, and the a or b axis of SBN tilts in-plane 18.4° away from the a axis of STO. This means SBN grows on STO in the manner of a unit cell match. Other than the cube-on-cube growth in perovskite, these growths are a kind of partially epitaxial growth. An eigen angle, 18.4° [arctg(1/3)], between a_{SBN} and a_{STO} is found in all models. The angle 18.4° can be calculated from relationship (2). This rotation angle results from the tilting between the octahedra in SBN and the vectors of the SBN unit cell. We note that a model similar to models 5 and 6 have been reported in Ref. 6–8. In the following section, we will compare the TEM results with our models.

B. Experimental results

Figure 2 shows the x-ray diffraction (XRD) pattern of SBN thin films on STO single crystals. Splitting can be seen in SBN (001) and SBN (002) peaks, which results from the overlap of SBN (001) and (002) peaks with (310) and (620) peaks, respectively. This result is in agreement with our models, in which the [001] and [130]/[310] zone axes are perpendicular to the film.

A bright-field image of a cross-section SBN film is shown in Fig. 3, which is taken near the [100] axis of STO substrate. Columnar grain structure is observed. Inside the grains, misfit dislocations and a few of threading dislocations are seen. Figure 4(a) shows a selected area diffraction (SAED) pattern from an area including one column and a part of substrate. It is indicated that the STO [100] zone axis accounts for the strong spots, and another pattern is from SBN [001] zone axis, which has a 18.4° rotation from STO [100]. Figure 4(b) is the pattern calculated by means the program JEMS based on model 1, which corresponds well with Fig. 4(a).[12] Figure 4(c) shows a SAED pattern taken on two grains as well as the substrate. Figure 4(c) includes two series of SBN [001] diffraction patterns, which indicate these two neighbor grains grow with the ⟨100⟩ zone axis rotated ±18.4° from the STO [100] zone-axis, as indicated in models 1 and 2, respectively.

The SAED pattern from another grain and substrate is shown in Fig. 5(a). Other than the STO [100] zone axis, it presents a [130] zone diffraction pattern of SBN as well
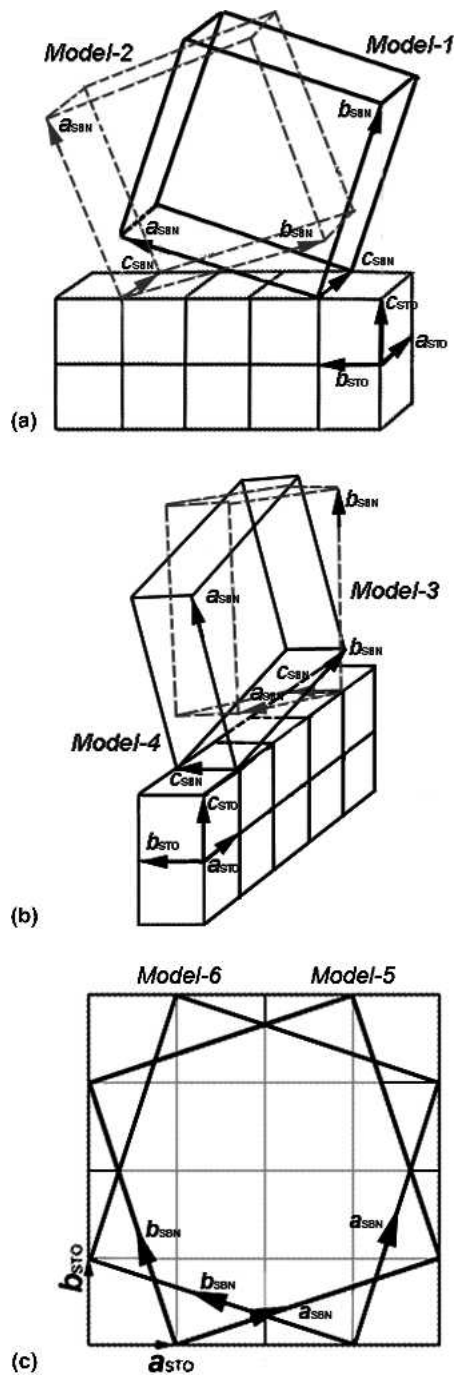
FIG. 1. Illustrations of the growth geometry of SBN on STO. (a) Model 1: [001]$_{SBN}$//[100]$_{STO}$, and [130]$_{SBN}$//[001]$_{STO}$ or a_{SBN} rotates −18.4° from b_{STO}; Model 2: [001]$_{SBN}$//[100]$_{STO}$, and [310]$_{SBN}$//[001]$_{STO}$ or a_{SBN} rotates (18.4–90°) from b_{STO}. Models 1 and 2 are seen along STO [100]. (b) Model 3: [001]$_{SBN}$//[010]$_{STO}$, and [130]$_{SBN}$//[001]$_{STO}$ or a_{SBN} rotates (18.4°-90°) from a_{STO}; Model 4: [001]$_{SBN}$//[010]$_{STO}$, and [310]$_{SBN}$//[001]$_{STO}$ a_{SBN} rotates −18.4° from a_{STO}. Models 3 and 4 are seen along STO [010]. (c) Model 5: [001]$_{SBN}$//[001]$_{STO}$, and [130]$_{SBN}$//[010]$_{STO}$ or a_{SBN} rotates +18.4° from a_{STO}; Model 6 [seen along STI(001)]: [001]$_{SBN}$//[001]$_{STO}$, and [$\bar{1}$30]$_{SBN}$//[010]$_{STO}$ or a_{SBN} rotates −18.4° from a_{STO}; Models 5 and 6 are seen on STO [001]. (+) indicates clockwise rotation, (−) indicates means counterclockwise rotation.
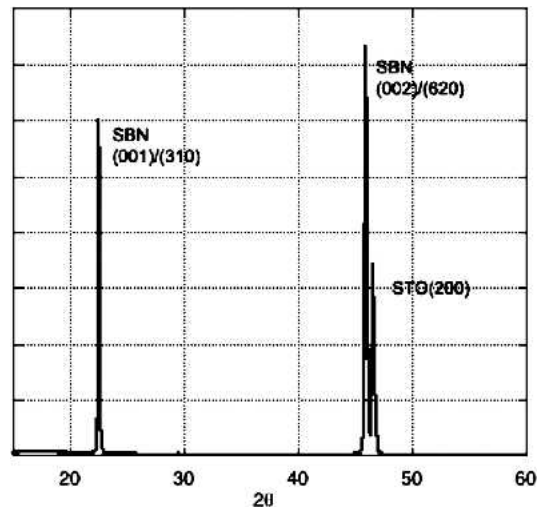

FIG. 2. XRD pattern of SBN thin film on (001) STO single crystal. SBN (001) and (002) peaks show splittings. The STO(200) peak shows no splitting.
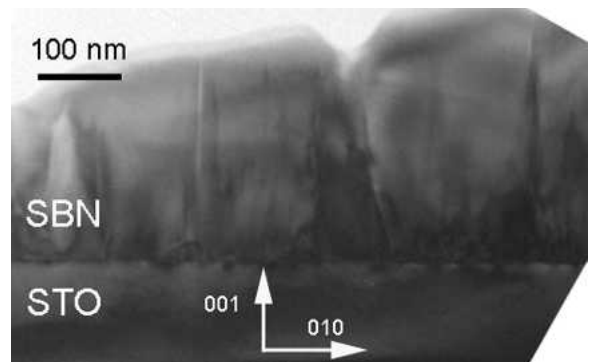

FIG. 3. Bright-field image of SBN thin film on STO substrate (cross-section).

as weak incommensurate superlattice reflections in plane (0, 0, h+1/2). Figure 5(b) is taken from both this grain and the adjacent grain. Besides the SBN [130] (or [310]) zone-axis pattern, both the incommensurate superlattice reflections and vertical SBN [$\bar{3}$10] (or [1$\bar{3}$0]) zone-axis pattern are observed. A corresponding schematic representation is shown in Fig. 5(c), where three sets of patterns in Fig. 5(b) are represented. First, the strong spots identical in Figs. 5(a) and 5(b) result from the grain with SBN [310] (or [130]) parallel with STO [001], indicated by filled circles. As simulated by JEMS, the (3k, −k, h) type spots are from reflections of the zero Laue-zone, and the (3k±1, −k, h) type spots are from reflections of the first Laue-zone. These spots indicate grain growth by models 3 and 4. Second, the vertical spots from the SBN [$\bar{3}$10] (or [1$\bar{3}$0]) zone-axis are from the adjacent grains with SBN[001] parallel to STO [001]. These spots indicate grain growth by models 5 and 6. Lastly, the streak-like spots are observed on (0, 0, h+1/2) planes. As reported in the literature,[13–15] these spots are incommensurate reflections induced by [NbO$_6$] octahedra tilting. It
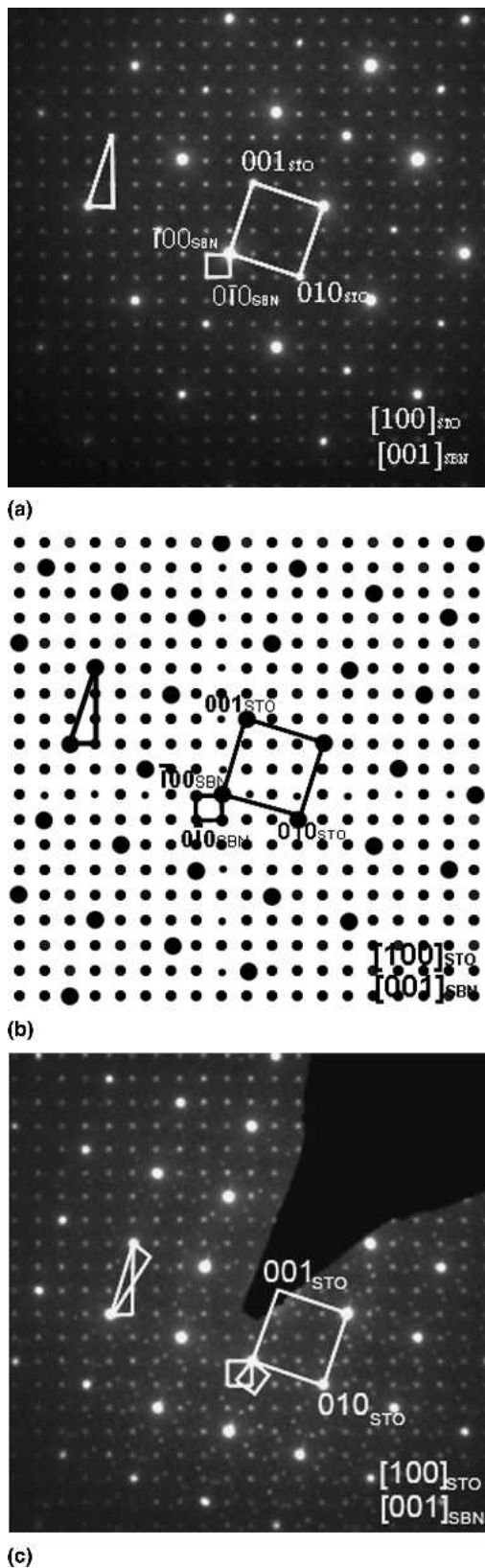
(a)

(b)

(c)

FIG. 4. (a) SAED pattern along STO[100] from a cross-section sample. The lattice units of SBN and STO are marked. (b) Calculated SAED pattern by JEMS. (c) SAED pattern along STO [100] from another area of the cross-section sample.
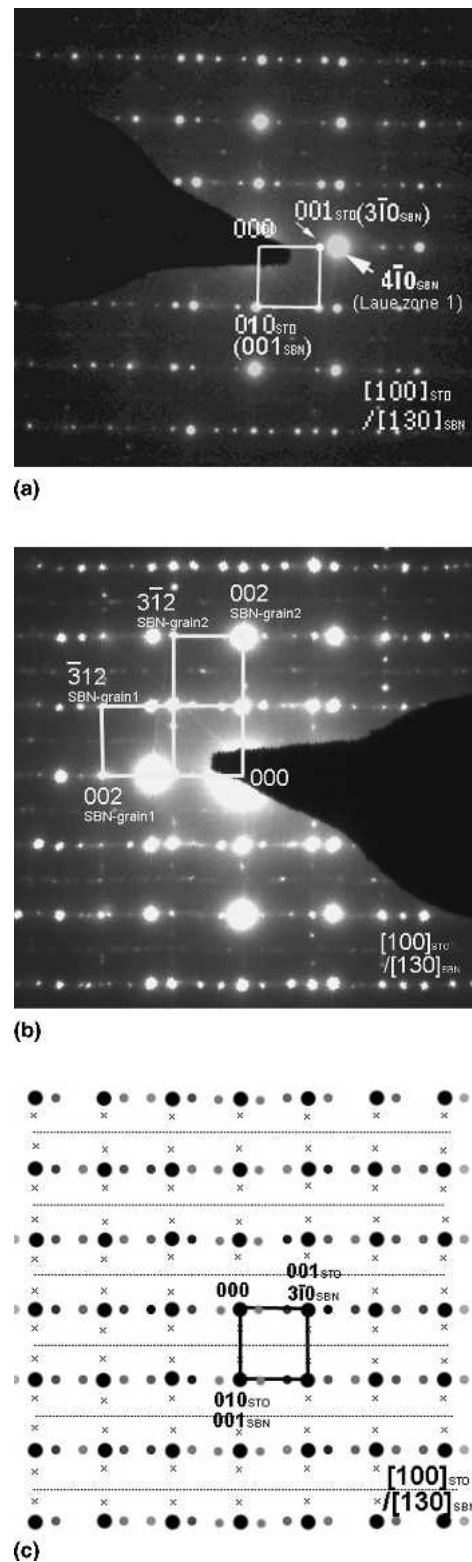

(a)

(b)

(c)

FIG. 5. (a) Cross-sectional SAED pattern of SBN/STO taken along STO [100]. (b) Cross-sectional SAED pattern from two grains. (c) Corresponding schematic representation of (a) and (b). The spots from the zero and first [130] Laue zones of SBN are respectively marked by large and small filled circles; the spots from adjacent grain are indicated by (×), and the spot-streaks of incommensurate reflections are indicated by (—).

is believed the incommensurate superlattice reflections suggest the SBN thin film is orthorhombic phase instead of tetragonal phase. In fact, the existence of (0, 0, h+1/2) superlattice reflections can help to distinguish the SBN [001] and SBN [130] zone axes, which have very similar diffraction patterns at the zero Laue zone.

Figure 6 is a HRTEM micrograph of a cross-section showing the boundary between two SBN grains. The fast Fourier transformations (FFT) on each grain are the same. The FFT pattern of Fig. 6 is shown in inset, where weak superlattice streaklike spots are observed. Therefore, it can be concluded that the two grains have the orientation relationship [001]$_{SBN}$//[001]$_{STO}$. Consequently, this boundary is an inverse (domain) boundary separating the two grains of models 5 and 6.

Figure 7 shows a HRTEM image of the film and substrate. Two SBN grains are observed with the growth relationships of [001]$_{SBN}$//[100]$_{STO}$ and [130]$_{SBN}$ or [310]$_{SBN}$//[001]$_{STO}$ (model 1 or 2) for grain one and [001]$_{SBN}$//[010]$_{STO}$, and [130]$_{SBN}$ or [310]$_{SBN}$//[001]$_{STO}$ (model 3 or 4) for grain two. Additionally, the angle between SBN[100] and STO [010] is measured as 18.4°, which confirms the observation in model 1.

TEM investigations were preformed on plane-view samples. A dark-field image from the plane-view is shown in Fig. 8(a). The STO substrate has been removed by ion milling, and only SBN grains are seen. Therein, two types of grains can be observed; one is platelike (bright), and the other is rodlike (dark). These grains are also seen in AFM observations (not shown). The inverse boundary separating the model 5 grain and the model 6

FIG. 7. HRTEM image of SBN thin film along STO [100] zone-axis showing the interface between SBN and STO.

grain can be observed. Figure 8(b) is the corresponding SAED pattern, in which two series of diffraction patterns correspond to the SBN [001] zone axis and one series of diffraction pattern corresponds to STO [001] zone axis. The patterns of two SBN [001] zone axes are from the planelike grains (models 5 and 6), and they have ±18.4° with the STO [001] zone axis, while the SBN [310]/[130] zone axis from the rodlike grains has the same pattern as STO [001]. These results are in agreement with the XRD pattern shown above, where strong SBN [001] and [130]/[310] peaks are reported.

With the help of diffraction simulation by JEMS, the grains of models 1–6 were identified by SAED and HRTEM.

C. Crystallographic models and discussion

From a crystallographic view, models 1–4 are equivalent, as are models 5 and 6. So it is crucial to discuss these six models at the atomic scale. STO is a typical perovskite with Ti in the center of oxygen octahedra (B-site) and Sr at the A site. Comparatively, the unit cell of SBN contains a framework of oxygen octahedral, and the tunnels among them are occupied by Sr and Ba ions. The bonds inside the oxygen octahedron are stable and difficult to break. Therefore, in the growth of SBN on STO, the octahedra structure will be adapted to maintain integrally and become the framework of growth. From the energy point of view, the octahedra of SBN would mainly overlap with the octahedra of STO to reduce the interface energy. According to these analyses and the six geometrical models shown previously, two crystallographic models are developed from the unit models of SBN and STO, as shown in Figs. 9(a) and 9(b), which
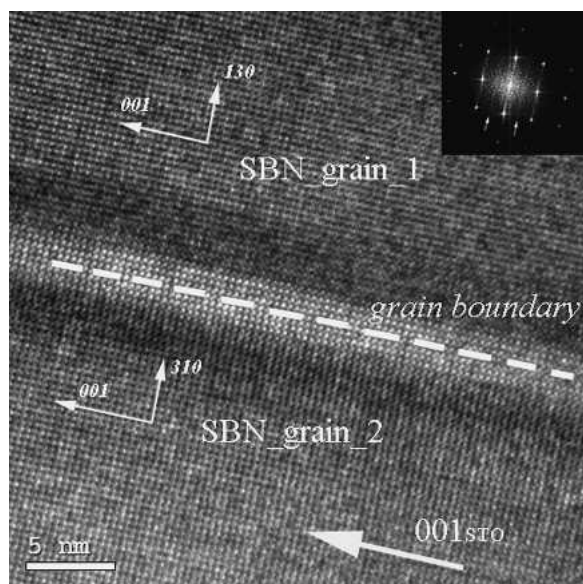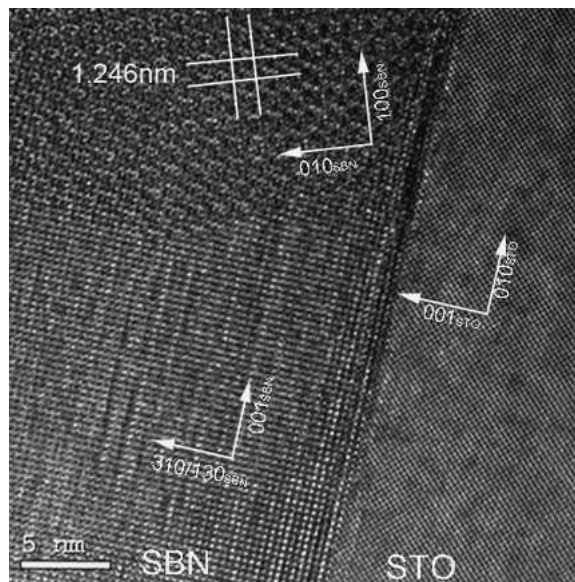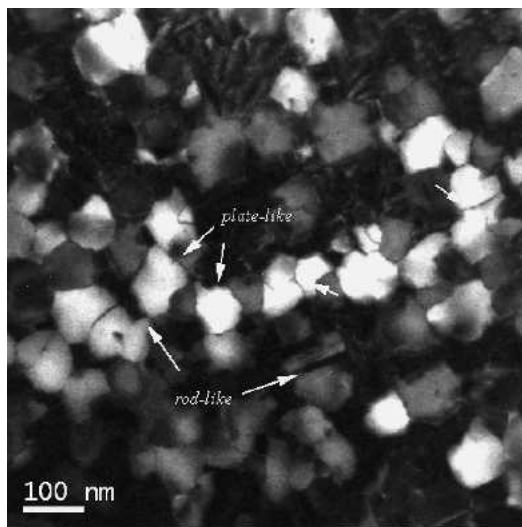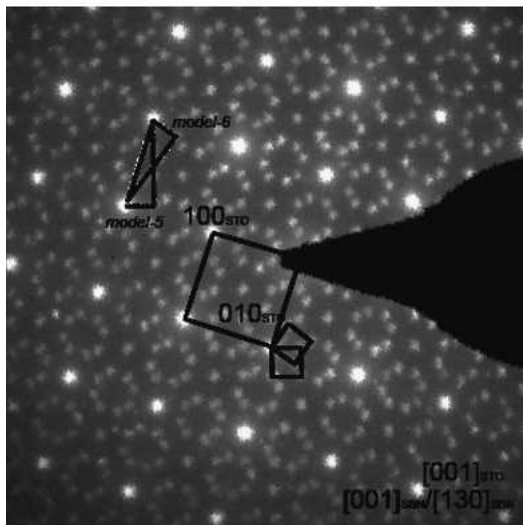

FIG. 6. HRTEM image of SBN thin film along the STO [100] zone-axis, showing the boundary of SBN grains. The inset is a FFT of HRTEM image, and the streaklike spots (0, 0, h+1/2) are marked with arrows.

(a)

(b)

FIG. 8. (a) Dark-field image from plane-view SBN thin film; (b) corresponding SAED pattern of (a).

(a)

(b)
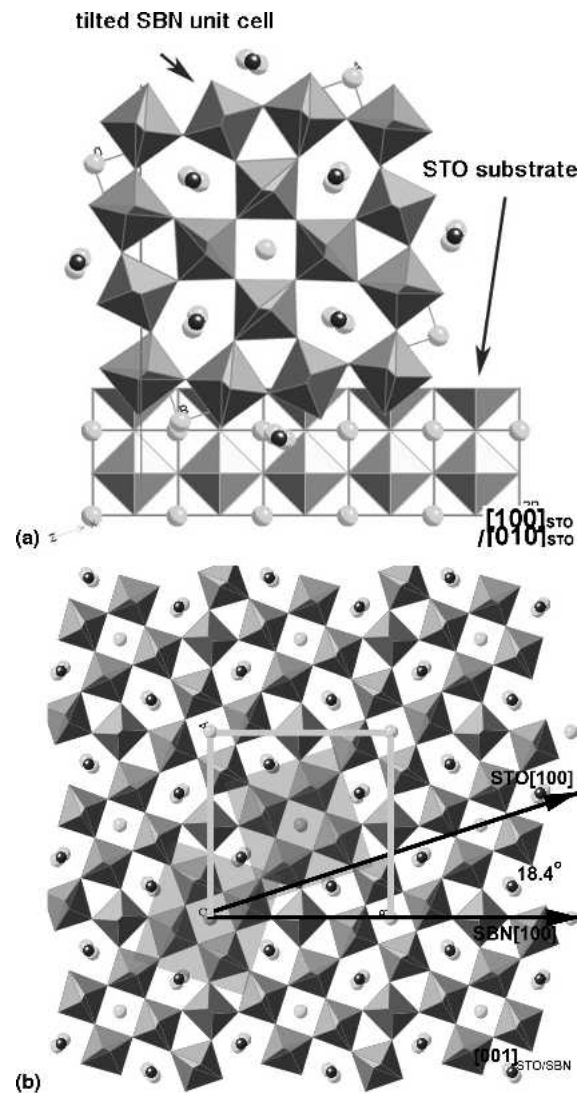
FIG. 9. Schematic graphs for SBN crystallographic growth on STO: (a) out-of-plane 18.4° rotation from STO and (b) in-plane 18.4° rotation from STO.

account for models 1–4 and models 5 and 6, respectively. One SBN unit cell has 10 octahedra on the boundary (shared with the neighboring unit cell) and 4 octahedra in the center. There is a relative rotation between them. Therefore, the maximal overlapping of octahedra between film and substrate can be achieved through two possible ways while keeping the growth epitaxial: In the case of Fig. 9(a), 4 oxygen octahedra on one side of the SBN unit cell boundary overlap maximally with the octahedra of the STO substrate. Figure 9(b) shows another case where the 4 octahedra in the center overlap maximally with the octahedra of STO.

From the growth models, it is indicated in Fig. 9(a) that growth has a different mismatch nature along the two directions on the interface between SBN and STO. The strains are 1.2% along a_{STO} and 0.9% along b_{STO}. In the

growth shown in Fig. 9(b), the strains are 0.9% along both a_{STO} and b_{STO}. [As mentioned above, at room temperature, the unit cell of SBN$_{x=0.5}$ should be an orthorhombic cell instead of the tetragonal cell that we used here. However, due to the lack of the knowledge on how the SBN slabs array (see Refs. 13 and 14), it is difficult to determine the realistic strain between the SBN and SBN. What we show here can be considered a reasonable estimation on the strain at high temperature.] The difference between strains along a and b directions is very small, which makes the different types of grains possible under the growth condition. The existence of dislocations can further relax strain in thin films and thus benefit the epitaxial growth of SBN film on STO single crystals.

Our models are based on the lattice parameters relationship between the SBN and STO. However, these

quasi-epitaxial models are not limited to these two particular materials, and these models can be applied to the epitaxial growth of tungsten-bronze thin film on other perovskite single crystal, such as MgO and LaAlO$_3$, within the tolerance of epitaxial growth. Most recently, Jia et al. studied the growth of another TB-type material Ca$_{1.4}$Ba$_{3.6}$Nb$_{10}$O$_{30}$ (Ca$_{0.28}$Ba$_{0.72}$Nb$_2$O$_6$ in their paper; CBN) on STO single crystals using an advanced negative Cs imaging technique.[16] The same growth patterns were found in the CBN/STO system, though the lattice mismatches in CBN/STO are 0.83% along a axes and 1.58% along c axes. Normally, the strain in thin film formed by PLD is strongly affected by various factors such as oxygen pressure, substrate temperature, pulse energy, quality of target, and film thickness. Therefore the growth nature of thin film is also affected. For example, the change of oxygen pressure can lead to the epitaxial growth of perovskite thin film varying from Frank–van Merwe (FM) (layer-by-layer) type to Volmer–Weber (VW) type. The identical models in SBN/STO and CBN/STO suggest that our current model is applicable to different stress state. We expect that the same growth model also works in SBN ceramics to reduce the internal strain.

We found that various conditions of surface treating to substrate can also affect the actual growth nature by changing the growth energy.[17] Other than the lattice-mismatch strain, the properties of the interface also play an important role in the epitaxial growth. This can be understood within the frame of the coincident site lattice approaches[16,18]; the surface treating can definitely influence the distribution of the atoms on the surface and lead to a change in the surface energy. In this case, an energy-favorable model will dominate the growth.

IV. CONCLUSIONS

In summary, TB-type SBN thin films were deposited on (001) SrTiO$_3$ single crystals. Based on relationships of the lattice parameters, six geometrical models of growth were built and a 18.4° rotation between film and substrate was found as a characteristic of this partially epitaxial growth. These results were confirmed by TEM. A kind of incommensurate superlattice reflection on (0, 0, h+1/2) was observed. Crystallographic models were produced to explain how SBN grows on STO. The lattice mismatches and surface chemical energy were found to play an important role in this quasi-epitaxial growth.

ACKNOWLEDGMENTS

REFERENCES

1. R.R. Neurgaonkar, J.R. Oliver, W.K. Cory, L.E. Cross, and D. Viehland: Piezoelectricity in tungsten bronze crystals. *Ferroelectrics* **160,** 265 (1994).
2. A.M. Glass: Investigation of the electrical properties of Sr$_{1-x}$Ba$_x$Nb$_2$O$_6$ with special reference to pyroelectric detection. *J. Appl. Phys.* **40**(12), 4699 (1999).
3. R.R. Neurgaonkar, R. Ratnakar, W.K. Cory, J.R. Oliver, M.D. Ewbank, and W.F. Hall: Development and modification of photorefractive properties in the tungsten bronze family crystals. *Opt. Eng.* **26**(5), 392 (1987).
4. P.D. Trivedi, P. Tayebati, and M. Tabat: Measurement of large electro-optic coefficients in thin films of strontium barium niobate (Sr$_{0.6}$Ba$_{0.4}$Nb$_2$O$_6$). *Appl. Phys. Lett.* **68,** 3227 (1996).
5. H-F. Cheng, G-S. Chiou, K-S. Liu, and I-N. Lin: Ferroelectric properties of (Sr$_{0.5}$Ba$_{0.5}$)Nb$_2$O$_6$ thin films synthesized by pulsed laser deposition. *Appl. Surf. Sci.* **113,** 217 (1997).
6. S.S. Thony, K.E. Youden, J.S. Harris, Jr., and L. Hesselink: Growth of epitaxial strontium barium niobate thin films by pulsed laser deposition. *Appl. Phys. Lett.* **65,** 2018 (1994).
7. C.M. Rouleau, G.E. Jellison, Jr., and D.B. Beach: Influence of MgO substrate miscut on domain structure of pulsed laser deposited Sr$_x$Ba$_{1-x}$Nb$_2$O$_6$ as characterized by x-ray diffraction and spectroscopic ellipsometry. *Appl. Phys. Lett.* **82,** 2990 (2003).
8. K. Tanaka, O. Nakagawara, M. Nakano, T. Shimuta, H. Tabata, and T. Kawai: Epitaxial growth of (Sr,Ba)Nb$_2$O$_6$ thin films by pulsed laser deposition. *Jpn. J. Appl. Phys.* **37,** 6142 (1998).
9. A. Infortuna, P. Muralt, M. Cantoni, A. Tagentsev, and N. Setter: Microstructural and electrical properties of (Sr,Ba)Nb$_2$O$_6$ thin films grown by pulsed laser deposition. *J. Eur. Ceram. Soc.* **24,** 1573 (2004).
10. B. Scheetz, D. Nelson, L. Zellmer, D. Smith: ICDD, Grant-in-Aid, Penn State University, University Park, PA (1988).
11. S.A. Howard, J.K. Yau, and H.U. Anderson: Structural characteristics of Sr$_{1-x}$La$_x$Ti$_{3+}$ as a function of oxygen partial pressure at 1400 °C. *J. Appl. Phys.* **65,** 1492 (1989) and Calculated from ICSD using POWD-12++ (1997).
12. P. Stadelmann: EMS—A software package for electron-diffraction analysis and HREM image simulation in material science. *Ultramicroscopy* **21,** 131 (1997).
13. J. Schneck, J.C. Toledano, R. Whatmore, and F.W. Ainger: Incommentsurate phases in ferroelectric tetragonal tungsten bronzes. *Ferroelectrics* **36,** 327 (1981).
14. L.A. Bursill and J.L. Peng: Incommentsurate superstructures and phase transition of strontium barium niobate (SBN). *Acta Crystallogr., Sect. B* **43,** 49 (1987).
15. H-Y. Lee and R. Freer: High-order incommentsurate modulations and incommentsurate superstructures in transparent Sr$_{0.6}$Ba$_{0.4}$Nb$_2$O$_6$(SBN40) ceramics. *J. Appl. Crystallogr.* **31,** 683 (1998).
16. C.L. Jia, J. Schubert, T. Heeg, S.B. Mi, H.Y. Chen, B. Joschko, M. Burianek, M. Muhlberg, and K. Urban: Tailoring the orientations of complex niobate films on perovskite substrates. *Acta Mater.* **54,** 2383 (2006).
17. A. Infortuna, P. Muralt, M. Cantoni, and N. Setter: Epitaxial growth of (SrBa)Nb$_2$O$_6$ thin films on SrTiO$_3$ single crystal substrate. *J. Appl. Phys.* **100,** 104110 (2006).
18. W. Bollmann: *Crystal Defects and Crystalline Interfaces* (Springer-Verlag, Berlin, Germany, 1970).